

Highly Reliable, Cost-effective and Temperature-stable Top-illuminated Avalanche Photodiode (APD) for 100G Inter-Datacenter ER4-Lite Applications

Jack Jia-Sheng Huang^{1,2}, H. S. Chang², Yu-Heng Jan^{2,1}, H. S. Chen², C. J. Ni², E. Chou², S. K. Lee² and Jin-Wei Shi³

¹Source Photonics, 8521 Fallbrook Avenue, Suite 200, West Hills, CA 91304, U.S.A.

²Source Photonics, No.46, Park Avenue 2nd Rd., Science-Based Industrial Park, Hsinchu, Taiwan

³Department of Electrical Engineering, National Central University, Zhongli, Taiwan

Keywords: Avalanche Photodiode, APD Photodetector, InGaAs/InAlAs APD, Top-Illumination APD, 100Gb/s Ethernet, 100G Datacenter, ER4, IEEE802.3.

Abstract: One of the key enablers for 100G ER4-Lite optical modules is 25G APD photodetector that can be employed in 30-40km optical links for inter-datacenter applications. In this paper, we demonstrate that a cost-effective top-illuminated InGaAs/InAlAs APD photodetector can be manufactured to meet stringent IEEE standard of 100G ER4-Lite. The 25G APD shows high bandwidth, high sensitivity with superb temperature stability of breakdown voltage. The APD photodetector also possesses excellent durability against harsh optical and electrical overload in both burst and continuous modes. Robust reliability performance based on aging conditions of 85-175°C has also been achieved with an activation energy of 1.18eV.

1 INTRODUCTION

Optical transmission for data center applications is increasingly popular for future interconnection within and between the cities (Bilal et al., 2013; Manzano et al., 2013; Basa, 2016). The Institute of Electrical and Electronics Engineers (IEEE) has developed various 802.3 standards for the 125m-40km optical links listed in Table I. Since 2007, the technological development on 40Gbit/s and 100Gbit/s applications have further accelerated (Caruso, 2007). Historically, the data center communications over 10km distance represented the mainframe. However, ER4 applications have recently gained significant traction due to its technological advantage in the 30-40km optical reach.

One of the main challenges for ER4 ethernet is to maintain undistorted optical signal over a long transmission distance. One way to achieve the long-distance transmission is to increase the output power from the laser emitter. However, there are several engineering tradeoffs associated with the higher power design including reliability, design complexity and processing cost (Connolly, 2002; Rinner et al., 2003; Huang et al., 2012). In this paper, we

demonstrate an alternative low-cost ER4 solution by employing high-sensitivity, high-speed top-illuminated 25G APD photodetector on the receiver side. Our data shows that it is feasible to attain low-cost manufacturing of 25G APD with well-rounded design-in aspects in bandwidth, sensitivity and reliability. The top-illuminated APD (Huang et al., 2016; Chen, et al., 2018) can bring advantages of low cost and simple fabrication compared to the bottom-illumination design (Nada et al., 2014; Nada et al., 2012). In addition, the 25G APD photodetector can achieve superb durability against harsh electrical and optical overload stress conditions as well as robust reliability performance.

Table 1: IEEE 802.3 standards for 40G/100G optical modules and fiber optics.

40G/100G Ethernet	Transmission Distance	Optical fiber
SR4	125m	Multi-mode fiber (MMF)
FR4 (CWDM4)	2km	Single-mode fiber (SMF)
LR4	10km	SMF
ER4 Lite / ER4	30km / 40km	SMF

2 EXPERIMENTAL

Figure 1 shows the conceptual schematics of the top-illuminated APD device structure. The epitaxial layers were grown by molecular beam epitaxy (MBE). From top to bottom, it is composed of the p⁺-InGaAs contact layer, p⁺-InP window layer, graded InGaAs/InAlAs, InGaAs absorption layer, p-doped InAlAs field control layer (~1x10¹⁸ cm⁻³), intrinsic InAlAs multiplication (M-) layer, and N⁺ InAlAs/InP contact layers. In order to shorten the avalanche delay time, a thin M-layer (~90 nm) is chosen in our device structure (Nada et al., 2015; Campbell et al., 2004). The detail of our epi-layer structure can be referred to our previous work (Huang et al., 2017; Chen et al., 2018).

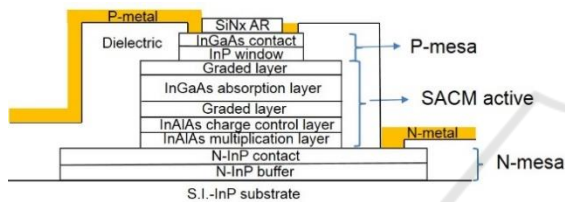


Figure 1: Schematics of top-illuminated mesa-type SACM APD photodetector structure with coplanar N and P electrodes.

We adopted the CH₄/H₂/Ar dry etching technique that exhibited a slow etching rate for the In_{0.52}Al_{0.48}As material in order to precisely control the depth of mesa etch. The active diameter of the APD device was about 20μm. After the mesa etch and p- and n-metal contacts, a thick (~5 μm) benzocyclobutene (BCB) film was used in the passivation process to reduce the dark current and to minimize the parasitic capacitance. An anti-reflection (AR) coating at 1.31 μm wavelength was deposited on the surface of our device to enhance its responsivity performance. A co-planar stripe (CPS) was integrated with our device for on-wafer high-speed measurement. The layout of our CPS was suitable for traditional wire bonding assembly of the top-illuminated APDs, bringing cost advantage compared to the flip-chip package that was used in some 25G bottom-illuminated APDs (Nada et al., 2015; Nada et al., 2014).

3 RESULTS AND DISCUSSION

3.1 Avalanche Breakdown Voltage

Figure 2 shows the typical reverse current-voltage (IV) curve of the 25G mesa-type SACM APD

photodetector. On the IV curve, there are two transitions along the reverse voltage that occur at 3V and 26V, respectively. The first transition at 3V corresponds to the punch-through voltage (V_{pt}) at which electric field depletes both the InAlAs multiplication and i-InGaAs absorption layers (Huang et al., 2017). The second transition represents the avalanche breakdown voltage (V_{br}) that is determined by the InAlAs multiplication layer. The avalanche breakdown voltage taken at 10μA is estimated to be about 26V for this device. The typical range of avalanche breakdown voltage is 24-26V. Our design allows excellent avalanche gain while keeping the tunneling and impact ionization away from the InGaAs absorption layer. The dark current refers to the reverse current at 0.9V_{br} is estimated to be about 13.4nA at 25°C.

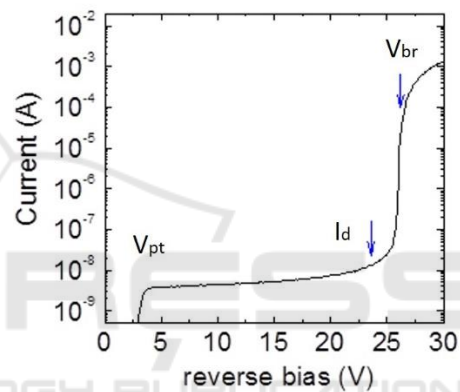


Figure 2: The reverse IV curve of the 25G APD photodetector where the first transition is related to the punch-through (V_{pt}) and the second related to the avalanche breakdown (V_{br}).

3.2 Bandwidth

Figure 3 shows the bandwidth plot of the APD based on small-signal modulation response at 25°C. We characterized the bandwidth curve at reverse voltage of 17V and 21V. At the reverse bias of 17V, the bandwidth taken by the 3dB roll-off reached 20GHz. Such bandwidth was adequate for meeting the requirement for 4x25G ER4 ethernet (Chen, et al., 2018). The corresponding multiplication factor or gain at -17V was about 2.2 (M=2.2). As the reverse bias increased to 21V for high gain operation (M=5), the 3dB bandwidth was maintained at around 15GHz.

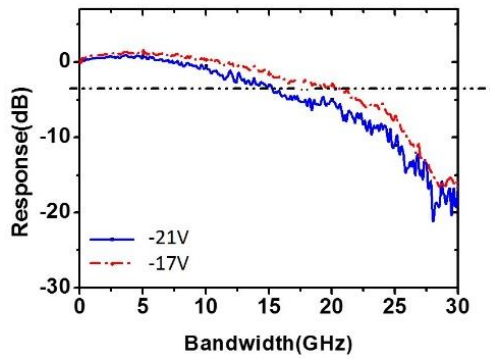


Figure 3: Bandwidth plot of 25G APD photodetector measured at 25°C with the reverse bias at 17V to BW of 20GHz.

3.3 Sensitivity

Figure 4 shows the bit error rate (BER) of the 25G APD photodetector as a function of input optical power. At near- V_{br} operation with gain of 6, the APD achieved error-free for bit error rate (BER) $<10^{-12}$, with the sensitivity of -17dBm. Such sensitivity level provided good margin for the photoreceiver detection over the 40km transmission over fiber (Laird et al., 2003; Alpert, 2015).

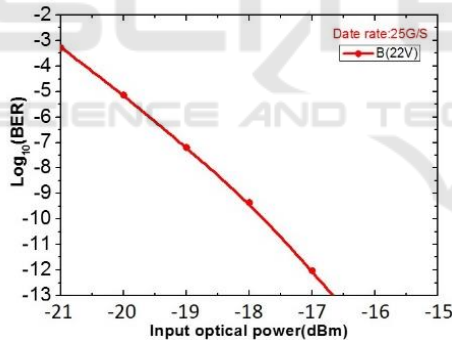


Figure 4: BER of 25G APD device showing that the sensitivity of -17dBm can be achieved for BER of 10^{-12} .

3.4 Temperature Stability

Temperature stability of the APD breakdown voltage is also an important parameter for ER4 datacenter applications. When the datacenter is running hot, the stable temperature stability of the APD would allow the gain to maintain constant when subject to temperature fluctuations.

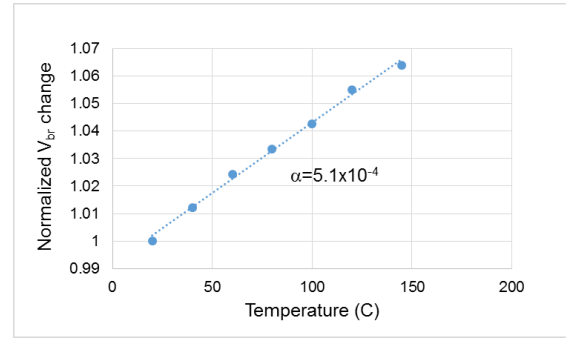


Figure 5: The normalized avalanche breakdown voltage of 25G APD as a function of temperature ranging from 25°C to 145°C.

The avalanche breakdown voltage followed a linear relationship with temperature (Tyagi, 1968), as shown in Equation (1).

$$V_{br}(T)/V_{br}(T_0) = 1 + \alpha(T - T_0) \quad (1)$$

where $V_{br}(T)/V_{br}(T_0)$ is the normalized avalanche breakdown voltage to the reference temperature T_0 and α is the normalized temperature coefficient. Figure 5 shows the normalized avalanche breakdown voltage as a function of temperature based on two different APD wafers. The normalized temperature coefficient (α) showed ultra-low value of about $5.1 \times 10^{-4} \text{C}^{-1}$, lower compared to the reported value of $7.2 \times 10^{-4} \text{C}^{-1}$ (Tan et al., 2010).

3.5 Optical & Electrical Overload Stress

In order to verify the photodetector's robustness against the simultaneous electrical and optical stresses, the mesa-type APD devices were tested with overload stress in burst and continuous modes, as illustrated in Fig. 6. To determine the damage threshold of overload, the optical stress was ramped up from -4dBm to +4dBm.

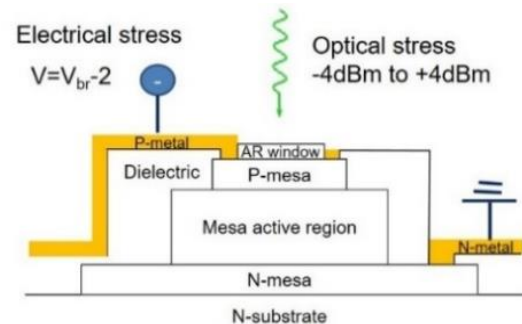


Figure 6: Schematic of electrical and optical overload stress applied to the APD for both burst and CW modes.

Table 2: Damage threshold of optical and electrical overload stresses of APD for burst and CW modes.

	Burst mode	CW mode
Damage threshold	No failure up to +4dBm.	No failure up to +1dBm.

In the burst mode, the optical stress of 1% pulsed duty cycle was applied to the APD for 60 seconds while the device was electrically stressed at 2V below V_{br} . All APD devices survived with no failure after being subjected to overload stress up to +4dBm, as shown in Table 2. In the continuous mode, the damage threshold was around +1dBm, well exceeding the -6dBm requirement.

3.6 Reliability

To establish long-term reliability performance, the APD devices were stressed at 85°C under a reverse current of 100µA (Telcordia, 2004). Figure 7 shows the relative change in avalanche breakdown voltage as a function of aging time. The failure criterion was defined as 1V change in V_{br} . All APD receivers have passed reliability test with excellent margin after 5100hr aging.

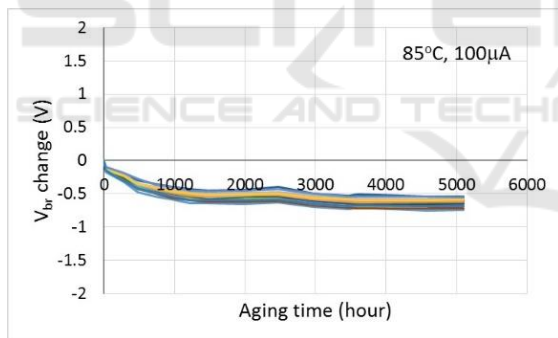


Figure 7: The relative breakdown voltage change as a function of aging time based on the stress condition of 85°C, 100µA.

Due to the small degradation at regular aging condition of 85°C, the APD devices were also stressed at highly elevated temperature. Figure 8 shows the failure time distributions of the APD from the aging groups of 165°C and 175°C. The failure time at 50% cumulative probability shows the statistical mean-time-to-failure (MTTF). The MTTF values for 165°C and 175°C are 896hrs and 446 hrs, respectively.

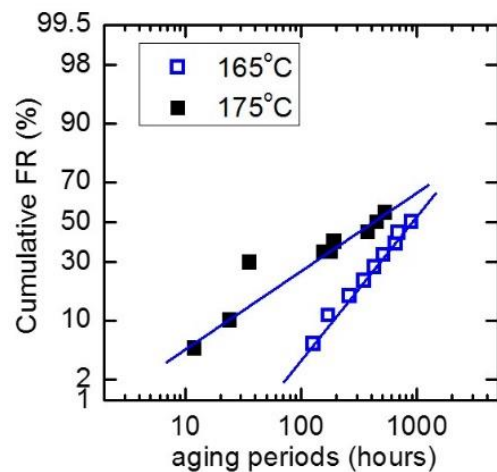


Figure 8: The failure time distributions of APD photodetectors based on the stress condition of 165°C and 175°C.

The device failure time (t_f) follows the modified Black’s equation (Black , 1969; Huang, 2005; Huang et al., 2005) which provides a good empirical description of device degradation over time as a function of stress current and temperature as shown in Equation (2).

$$t_f = \frac{A}{I^N} \exp\left(\frac{E_a}{kT}\right) \quad (2)$$

In Equation (2), the first term represents the current acceleration factor where A is a constant, I is the stress current, and N is the current exponent; the second term represents the temperature acceleration where E_a is the activation energy, k is the Boltzmann’s constant, and T is the temperature.

For the sake of activation energy study, Equation (2) can be rewritten in the form of natural logarithm as shown in Equation (3) where the third term can readily determine the activation energy.

$$\ln(MTTF) = \ln(A) - N \cdot \ln(I) + \frac{E_a}{kT} \quad (3)$$

Figure 9 shows the plot of $\ln(MTTF)$ vs. $1/(kT)$ where the slope is equal to E_a . The error bars indicates the variation between devices. Based on the experimental aging data of 165°C and 175°C, the E_a of APD is estimated to be 1.18eV, in close agreement with other reported values (Ishimura et al., 2007; Watanabe et al., 1996).

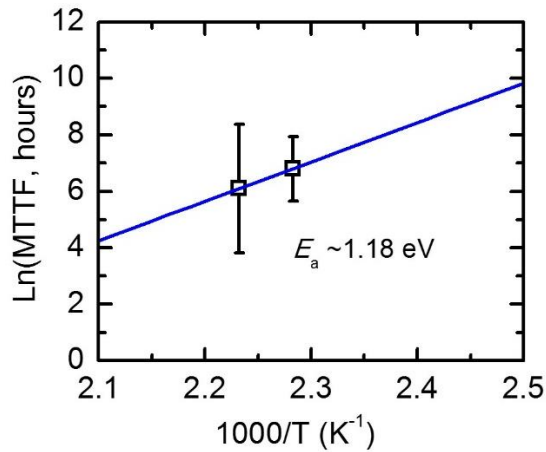


Figure 9: The plot of Ln(MTTF) vs. $1/(kT)$ for the determination of E_a . The E_a value was 1.18eV.

Table 3: Projected device lifetimes of mesa-type APD at 50°C operating condition based on extrapolation from the stress condition.

Aging stress temperature	Failure time at stress temperature	Device operating lifetime at 50°C
165°C	896 hours	6912 years
175°C	446 hours	6909 years

With the E_a establishment, the failure times from the aging test can be extrapolated to project the device lifetimes at the operating condition by using Equation (2). For the 50°C operating condition, the device lifetimes of the 25G APD are estimated to be close to 6900 years shown in Table 3, representing great reliability margin for the 20-year stringent requirement per Telcordia.

4 CONCLUSIONS

We have demonstrated low-cost manufacturing of 25G top-illuminated, high-sensitivity SACM APD photodetector for the 100G ER4 Lite datacenter applications. The high-speed, high-sensitivity APD showed favorable V_{br} (24-26V). The 3dB bandwidth reached 20GHz at reverse bias of 17V, meeting the requirement of 4x25G ER4 ethernet. The sensitivity of -17dBm was achieved to enable the detection over the error-free 40km transmission over fiber at $BER < 10^{-12}$. The APD also showed excellent temperature stability where the normalized

temperature coefficient (α) was about $5.1 \times 10^{-4} \text{ }^\circ\text{C}^{-1}$, superior to the industry benchmark.

The APD photodetector showed superb durability against simultaneous electrical and optical overload stress. In the burst mode, the APD showed no failure up to +4dBm. In the CW mode, the damage threshold was +1dBm, well exceeding the -6dBm requirement. We have also achieved robust reliability for the APD with little degradation after 5100hr aging at 85°C. Based on the aging data of 165°C and 175°C, the activation energy of the APD was determined to be 1.18eV. The projected device lifetime of the APD was extrapolated to be about 6900 years at the operating condition of 50°C.

REFERENCES

- Bilal, K., Khan, S.U. and Zomaya, A.Y., "Green data center networks: challenges and opportunities", *11th Int'l Conf. on Frontiers of Information Technology (FIT)*, p.229-234, (Islamabad, Pakistan, 2013).
- Manzano, M., Bilal, K., Calle, E., and Khan, S. U., "On the connectivity of data center networks," *IEEE Comm. Lett.*, vol. 17, no. 11, p. 2172-2175, (2013).
- Basa, J., "Source Photonics announces shipment of 10,000 single mode 100G QSFP28 modules", *Optical Fiber Communications Conference (OFC, Anaheim, CA, 2016)*.
- Caruso, J., "Group pushes 100 Gigabit ethernet: the "Road to 100G" alliance is born", *Network World*, (June 21, 2007).
- Connolly, M. J., "*Semiconductor Optical Amplifiers*", (Springer-Verlag, Boston, MA, 2002).
- Rinner, F., Rogg, J., Kelemen, M., and Poprawe, R., "Facet temperature reduction by a current blocking layer at the front facets of high-power InGaAs/AlGaAs lasers", *J. Appl. Phys.*, vol.93, no.3, p.1848-1850, (2003).
- Huang, J.S., Isip, E., and Carson, R.F. "High-resolution wavelength stability aging study of C-band 100mW high-power DWDM laser modules", *IEEE Photon. Conf. (Burlingame, CA, 2012)*, p.538-539.
- Huang, M., Cai, P., Li, S., Wang, L., Su, T.-I., Zhao, L., Chen, W., Hong, C.-Y., and Pan, D., "Breakthrough of 25Gb/s Germanium on Silicon Avalanche Photodiode", *Optical Fiber Communications Conf.*, OFC Technical Digest, (Anaheim, CA, 2016), Paper Tu2D.2.
- Chen, Y.H., Wun, J.M., Wu, S.L., Huang, J.S., Jan, Y.H., Chang, H.S., Chen, H.S., Ni, C.J., Chou, E. and Shi, J.W., "Top-illuminated In_{0.52}Ga_{0.48}As based avalanche photodiode with dual charge layers for high-speed and low dark current performances", *IEEE J. Select. Topic. Quantum Electronics*, vol.24, no.2, p.3800208, (2018).
- Nada, M., Muramoto, Y., Yokoyama, H., and Matsuzaki, H., "High-speed high-power-tolerant avalanche photodiode for 100-Gb/s applications", *IEEE Photonic Conf.*, (San Diego, CA, 2014), p.172-173.

- Nada, M., Muramoto, Y., Yokoyama, H., Ishibashi, T., and S. Kodama, "InAlAs APD with high multiplied responsivity-bandwidth product (MR-bandwidth product) of 168 A/W.GHz for 25 Gbit/s high-speed operations", *Electron. Lett.*, vol. 48, no. 7, pp. 397-399, (2012).
- Nada, M., Yoshimatsu, T., Muramoto, Y., Yokoyama, H. and Matsuzaki, H., "Design and Performance of High-Speed Avalanche Photodiodes for 100-Gb/s Systems and Beyond," *IEEE/OSA Journal of Lightwave Technology*, vol. 33, no. 5, pp. 984-990, (2015).
- Campbell, J. C., Demiguel, S., Ma, F., Beck, A., Guo, X., Wang, S., Zheng, X., Li, X., Beck, J. D., Kinch, M. A., Huntington, A., Coldren, L. A., Decobert, J. and Tschertner, N., "Recent Advances in Avalanche Photodiodes," *IEEE J. of Sel. Topics in Quantum Electronics*, vol. 10, pp. 777-787, (2004).
- Huang, J.S., Chang, H.S., Jan., Y.H., Ni, C.J., Chen, H.S., and Chou, E., "Temperature dependence study of mesa-type InGaAs/InAlAs avalanche photodiode characteristics", *Adv. Optoelectron.*, no. 2084621, p.1-5, (2017).
- Laird, J.S., Hirao, T., Onoda, S., Ohyama, H., and T. Kamiya, T., "Heavy-ion induced single-event transients in high-speed InP-InGaAs avalanche photodiodes", *IEEE Tran. Nuclear Sci.*, Vol. 50, No. 6, p.2225-2232, (2003).
- Alpert, A., "High-speed jitter testing of XFP transceivers", Viavi White Paper, (2015).
- Tyagi, M.S., "Zener and avalanche breakdown in silicon alloyed p-n junctions" *Solid State Electron.*, vol. 11, p.99-128, (1968).
- Tan, L.L. J., Ong, D.S.G., Ng, J.S., Tan, C.H., Jone, S.K., Qian Y., and David, J.P.R., "Temperature dependence of avalanche breakdown in InP and InAlAs", *IEEE J. Quantum. Electron.*, vol.46, no.8, p.1153-1157, (2010).
- "Generic reliability assurance requirements for optoelectronic devices used in telecommunication equipment", Telcordia, GR-468-CORE, (2004).
- Black, J.R., "Electromigration failure modes in aluminum metallization for semiconductor devices", *Proc. IEEE*, vol.57, no.9, p.1587-1594, (1969).
- Huang, J.S., "Temperature and current dependences of reliability degradation of buried heterostructure semiconductor lasers", *IEEE Tran. Device Mater. Reliab. Vo.5, no.1, p.150-154, (2005).*
- Huang, J.S., Nguyen, T., Hsin, W., Aeby, I., Ceballo, R., and Krogen, J., "Reliability of etch-mesa buried heterostructure semiconductor lasers", *IEEE Tran. Device Mater. Reliab. Vo.5, no.4, p.665-674, (2005).*
- Ishimura, E., Yagy, E., Nakaji, M., Ihara, S., Yoshiara, K., Aoyagi, T., Tokuda, Y., and Ishikawa, T., "Degradation mode analysis on highly reliable guardring-free planar InAlAs avalanche photodiodes", *J. Lightwave Tech.*, vol. 25, no. 12, p.3686-3693, (2007).
- Watanabe, I., Tsuji, M., Hayashi, M., Makita K., and Taguchi, K., "Reliability of Mesa-Structure InAlGaAs-InAlAs superlattice avalanche photodiodes", *IEEE Photonics Tech. Lett.*, Vol. 8, No. 6, p.824-826, (1996).